

The ASAS-SN Catalog of Variable Stars VII: Contact Binaries are Different Above and Below the Kraft Break

T. Jayasinghe^{1,2*}, K. Z. Stanek^{1,2}, C. S. Kochanek^{1,2}, B. J. Shappee³,
M. H. Pinsonneault¹, T. W. -S. Holoien⁴, Todd A. Thompson^{1,2,5}, J. L. Prieto^{6,7},
M. Pawlak⁸, O. Pejcha⁸, G. Pojmanski⁹, S. Otero¹⁰, N. Hurst¹¹, D. Will^{1,11}

¹Department of Astronomy, The Ohio State University, 140 West 18th Avenue, Columbus, OH 43210, USA

²Center for Cosmology and Astroparticle Physics, The Ohio State University, 191 W. Woodruff Avenue, Columbus, OH 43210, USA

³Institute for Astronomy, University of Hawaii, 2680 Woodlawn Drive, Honolulu, HI 96822, USA

⁴Carnegie Observatories, 813 Santa Barbara Street, Pasadena, CA 91101, USA

⁵Institute for Advanced Study, Princeton, NJ, 08540

⁶Núcleo de Astronomía de la Facultad de Ingeniería y Ciencias, Universidad Diego Portales, Av. Ejército 441, Santiago, Chile

⁷Millennium Institute of Astrophysics, Santiago, Chile

⁸Institute of Theoretical Physics, Faculty of Mathematics and Physics, Charles University, Czech Republic

⁹Warsaw University Observatory, Al Ujazdowskie 4, 00-478 Warsaw, Poland

¹⁰The American Association of Variable Star Observers, 49 Bay State Road, Cambridge, MA 02138, USA

¹¹ASC Technology Services, 433 Mendenhall Laboratory 125 South Oval Mall Columbus OH, 43210, USA

Accepted XXX. Received YYY; in original form ZZZ

ABSTRACT

We characterize $\sim 71,200$ W UMa type (EW) contact binaries, including $\sim 12,600$ new discoveries, using ASAS-SN V-band all-sky light curves along with archival data from Gaia, 2MASS, AllWISE, LAMOST, GALAH, RAVE, and APOGEE. There is a clean break in the EW period-luminosity relation at $\log(P/d) \simeq -0.30$, separating the longer period early-type EW binaries from the shorter period, late-type systems. The two populations are even more cleanly separated in the space of period and effective temperature, by $T_{\text{eff}} = 6710 \text{ K} - 1760 \text{ K} \log(P/0.5 \text{ d})$. Early-type and late-type EW binaries follow opposite trends in T_{eff} with orbital period. For longer periods, early-type EW binaries are cooler, while late-type systems are hotter. We derive period-luminosity relationships (PLRs) in the W_{JK} , V , Gaia DR2 G , J , H , K_s and W_1 bands for the late-type and early-type EW binaries separated both by period and effective temperature, and by period alone. The dichotomy of contact binaries is almost certainly related to the Kraft break and the related changes in envelope structure, winds and angular momentum loss.

Key words: stars:variables –stars:binaries:eclipsing – catalogues –surveys

1 INTRODUCTION

Contact binaries are close binary systems whose components fill their Roche Lobes. The most abundant are the W Ursae Majoris (W UMa) variables that are characterized by having nearly equal primary and secondary eclipse depths and orbital periods of $\sim 0.2 - 1$ d. Given that both stars overflow their Roche lobes, the orbital periods of W UMa variables are closely related to the mean stellar densities (Eggleton 1983). As a result, these contact binaries follow a period-luminosity relation, which can yield distances accurate to 10% (Rucinski 1994; Chen et al. 2016, 2018). W UMa variables show little color variability and similar eclipse depths, so the component stars have similar effective temperatures and are in thermal contact (Webbink 2003). In most variable star catalogues, W UMa variables are assigned the GCVS/VSX (Samus et al. 2017; Watson et al. 2006) classification of ‘EW’.

W UMa variables are abundant in the Galaxy, and the advent of

wide field surveys, such as the All-Sky Automated Survey (ASAS; Pojmanski 2002), the Optical Gravitational Lensing Experiment (OGLE; Udalski 2003), the Northern Sky Variability Survey (NSVS; Woźniak et al. 2004), MACHO (Alcock et al. 1997), EROS (Derue et al. 2002), the Catalina Real-Time Transient Survey (CRTS; Drake et al. 2014), the Asteroid Terrestrial-impact Last Alert System (ATLAS; Tonry et al. 2018; Heinze et al. 2018), have yielded $\geq 10^5$ such variables. Using the ASAS catalog, Rucinski (2006) estimated an abundance relative to FGK stars of 0.2%. Given their high occurrence rates, they can also be used to study Galactic structure (Rucinski 1997).

Contact binaries play a significant role in stellar evolution and maybe the progenitors for objects such as blue stragglers (Andronov et al. 2006; Chen, & Han 2009) and Oe/Be stars (Eggleton 2010; de Mink et al. 2013). In one case, a contact binary was observed to evolve into a stellar merger (Tylenda et al. 2011). Thus, the study of the formation and evolution of contact binaries will improve our understanding of binary mergers and stellar evolution.

The detached-binary channel is considered to be crucial for the

* E-mail: jayasinghearachilage.1@osu.edu

formation of contact binaries (Rucinski 1986; Li et al. 2007; Jiang et al. 2014). In this channel, a close detached binary evolves to Roche lobe overflow and then to contact either through the evolutionary expansion of the components (Webbink 1976) or through angular momentum loss by magnetic braking (Vilhu 1982). Studies of chromospherically active binaries have shown that they are losing angular momentum and evolving towards shorter orbital periods, making them good candidates for the progenitors of contact binaries (Eker et al. 2006). Paczyński et al. (2006) studied the eclipsing binaries in the ASAS catalog and noted a deficiency of close detached binaries with periods $P < 1$ d compared to the number needed to produce the observed number of contact binaries. It seems likely that many contact binaries form in triple systems, where the Kozai-Lidov mechanism (Lidov 1962; Kozai 1962) drives the evolution towards becoming contact binaries (Eggleton, & Kiseleva-Eggleton 2001). The formation time-scale of contact binaries from a single starburst in the detached-binary channel has a large dynamic range (~ 1 Myr to ~ 15 Gyr, Jiang et al. 2014), which can explain the existence of very young contact binaries (< 10 Myr) (Van Eyken et al. 2011).

W UMa contact binaries are observationally classified into A-type and W-type systems. The primary eclipse in the A-type systems corresponds to the transit of the secondary across the primary, whereas W-type systems are those whose secondaries are occulted by the primary. The sub-types also have different spectral types. A-type systems have A-F spectra and W-type systems have G-K spectra (Webbink 2003). Thus, the two sub-types appear to be separated in temperature, with A-type systems having temperatures ≥ 6000 K (Rucinski 1974). The massive component of an A-type system is hotter than the less massive component and the opposite is true for W-type systems (Yildiz & Doğan 2013; Binnendijk 1970). The formation mechanism of A-type contact binaries in the pre-contact phase is dominated by the nuclear evolution of the more massive component ($1.8M_{\odot} < M < 2.7M_{\odot}$) and the angular momentum evolution of the less massive component ($0.2M_{\odot} < M < 1.5M_{\odot}$) (Yildiz 2014). The pre-contact phases for the A-type systems typically end as the primary begins to evolve off the main-sequence. In the W-type systems, both components undergo efficient angular momentum loss and in most cases the angular momentum evolution is so rapid that the binary evolves into contact before the primary leaves the main-sequence (Yildiz 2014). In this work, we will refer to the A-type systems as early-type EW binaries and the W-type systems as late-type EW binaries. The early/late types are related to the W/A sub-types but the classifications are not completely identical.

Main-sequence stars follow two distinct rotational regimes that are determined by how efficiently the stars lose angular momentum. Stars cooler than $T_{\text{eff}} \lesssim 6200$ K are slow rotators (Van Saders, & Pinsonneault 2013). These stars have thick convective envelopes, and rapidly lose their angular momentum due to magnetized winds. Hot stars with $T_{\text{eff}} \gtrsim 6700$ K rotate rapidly (Royer et al. 2007) because they do not have thick convective envelopes, and angular momentum loss through magnetized winds becomes very inefficient. The transition from the slowly-rotating main-sequence stars to the rapidly rotating main-sequence stars occurs at $\sim 1.3M_{\odot}$ (early F spectral types) and is known as the Kraft break (Kraft 1967). The differences in angular momentum loss above and below the Kraft break, presumably drive the evolutionary difference between the early and late-type binaries.

In a series of papers, Jayasinghe et al. (2018, 2019b,d,e,c), we have been systematically identifying and classifying variables using data from The All-Sky Automated Survey for SuperNovae (ASAS-SN, Shappee et al. 2014; Kochanek et al. 2017). We have thus far discovered $\sim 220,000$ new variables and homogeneously classified both the new and previously known variables in the sample (Jayas-

inghe et al. 2019a). Here, we analyze an all-sky catalogue of 71242 W UMa (EW) contact binaries in the ASAS-SN V-band data. In Section §2, we summarize the ASAS-SN catalogue of EW binaries and the cross-matching to external photometric and spectroscopic catalogues. We analyze the sample of EW binaries with spectroscopic cross-matches and compare early-type and late-type systems in Section §3. We derive period-luminosity relationships for these two sub-types in Section §4. The V-band light curves and other variability and photometric information for all of the $\sim 71,200$ sources studied in this work are available online at the ASAS-SN variable stars database (<https://asas-sn.osu.edu/variables>).

2 THE ASAS-SN CATALOG OF CONTACT BINARIES

In this work, we selected 71242 W UMa-type contact binary stars (EW) identified during our systematic search for variables, including new EW binaries in the Northern hemisphere and regions of the southern Galactic plane that were missed in the previous survey papers (Jayasinghe et al. 2020, in prep). Out of the 71242 EW binaries in this catalogue, 12584 ($\sim 18\%$) are new ASAS-SN discoveries. The ASAS-SN V-band observations used in this work were made by the “Brutus” (Haleakala, Hawaii) and “Cassius” (CTIO, Chile) quadruple telescopes between 2013 and 2018. Each ASAS-SN V-band field is observed to a depth of $V \lesssim 17$ mag. The field of view of an ASAS-SN camera is 4.5 deg^2 , the pixel scale is $8''0$ and the FWHM is typically ~ 2 pixels. ASAS-SN saturates at $\sim 10 - 11$ mag, but we attempt to correct the light curves of saturated sources for bleed trails (see Kochanek et al. 2017). The V-band light curves were extracted as described in Jayasinghe et al. (2018) using image subtraction (Alard & Lupton 1998; Alard 2000) and aperture photometry on the subtracted images with a 2 pixel radius aperture. The APASS catalog (Henden et al. 2015) and the ATLAS All-Sky Stellar Reference Catalog (Tonry et al. 2018) were used for calibration. We corrected the zero point offsets between the different cameras as described in Jayasinghe et al. (2018). The photometric errors were recalculated as described in Jayasinghe et al. (2019b).

Variable sources were identified and subsequently classified using two independent random forest classifiers plus a series of quality checks as described in Jayasinghe et al. (2019a,d). We used the *astropy* implementation of the Generalized Lomb-Scargle (GLS, Zechmeister & Kürster 2009; Scargle 1982) periodogram and the *astrobases* implementation (Bhatti et al. 2018) of the Box Least Squares (BLS, Kovács et al. 2002) periodogram, which improves the completeness for eclipsing binaries, to search for periodicity over the range $0.05 \leq P \leq 1000$ days. We classified the eclipsing binaries into the GCVS/VSX photometric (sub-)classes: EW, EB and EA. EW (W UMa) binaries have light curves with minima of similar depths whereas EB (β -Lyrae) binaries tend to have minima of significantly different depths. The ratio of eclipse depths (D_s/D_p) for most contact binaries are $D_s/D_p > 0.8$, whereas most semi-detached systems have eclipses of different depths with $D_s/D_p < 0.8$ (Paczyński et al. 2006; Jayasinghe et al. 2019a). Most contact binaries are in thermal contact, but Paczyński et al. (2006) also noted systems with unequal minima, implying that some contact binaries are not in thermal contact, as was predicted by models of thermal relaxation oscillations (see, for e.g., Lucy 1976; Flannery 1976; Yakut & Eggleton 2005). Both the EW (contact) and EB (contact/semi-detached) binaries transition smoothly from the eclipse to the out-of-eclipse state. EA (Algol) binaries are detached systems where the exact onset and end of the eclipses are easily defined. These detached systems may or may not have a secondary minimum.

We cross-matched the EW binaries with Gaia DR2 (Gaia Collaboration et al. 2018a) using a matching radius of $5''$. The sources were assigned distance estimates from the Gaia DR2 probabilistic distance estimates (Bailer-Jones et al. 2018) by cross-matching based on the Gaia DR2 `source_id`. A large majority of these sources ($\sim 86.8\%$) had distance estimates from Gaia DR2. We also cross-matched these sources to the 2MASS (Skrutskie et al. 2006) and AllWISE (Cutri et al. 2013; Wright et al. 2010) catalogues using a matching radius of $10''$. We used TOPCAT (Taylor 2005) for this process. Following the cross-matching process, we calculated the absolute, reddening-free Wesenheit magnitude (Madore 1982; Lebzelter et al. 2018) for each source as

$$W_{JK} = M_{K_s} - 0.686(J - K_s). \quad (1)$$

For each source, we also calculate the total line of sight Galactic reddening $E(B-V)$ from the recalibrated ‘SFD’ dust maps (Schlafly & Finkbeiner 2011; Schlegel et al. 1998).

We cross-matched our sample with the APOGEE DR15 catalog (Holtzman et al. 2015; Majewski et al. 2017), the RAVE-on catalog (Casey et al. 2017), the LAMOST DR5 v4 catalog (Cui et al. 2012) and the GALAH DR2 catalog (De Silva et al. 2015; Buder et al. 2018) using a matching radius of $5''$. We identified 7169 matches to the EW binaries from the LAMOST (94.0%), GALAH (3.8%), RAVE (2.1%) and APOGEE (0.1%) spectroscopic surveys.

The median V-band magnitude of the EW binary sample is $V \sim 14.7$ mag. Classification probabilities of $\text{Prob} > 0.9$ are considered very reliable and $\sim 93.4\%$ of our sample of contact binaries have $\text{Prob} > 0.9$. There are 21837 sources within 1 kpc but a considerable fraction ($\sim 69\%$) of the sources with Gaia DR2 distances are located further away. A large fraction have useful parallaxes, as $\sim 69\%$ ($\sim 58\%$) of the sources have $\text{parallax}/\text{parallax_error} > 5$ (> 10). The median line-of-sight extinction to the EW binaries is $A_V \sim 0.36$ mag, assuming $R_V = 3.1$ dust (Cardelli et al. 1989). The sky distribution of the EW binaries in ASAS-SN, colored by their period, is shown in Figure 1.

We present the ASAS-SN light curves for 10 late-type and 10 early-type contact binaries to illustrate the light curve morphologies of these systems. The phased ASAS-SN V- and g-band light curves are shown in Figure 2 (late-type EW) and Figure 3 (early-type EW). The ratio of eclipse depths is similar for both the late-type and early-type binaries. We do not see substantial differences in the morphologies of the light curves between early-type and late-type contact binaries. The variations in the depths of the minima are generally only a few percent (Webbink 2003), making it challenging to distinguish the early and late-type systems using the ASAS-SN light curves.

The period distribution of the EW binaries is shown in Figure 4. The EW binaries have a bimodal orbital period distribution, with the late-type systems (canonically defined as those with $\log(P/d) < -0.25$) having a median period of $\log(P/d) \sim -0.4$, and the early-type systems having a median period of $\log(P/d) \sim -0.15$. Most sources with periods $P > 1$ d are likely β -Lyrae eclipsing binaries (EB), with nearly equal minima that are misclassified as contact (EW) binaries. We will discuss the differences between early-type and late-type contact binaries in Section §3 and derive period-luminosity relationships for these two sub-types in Section §4.

3 EARLY-TYPE VS. LATE-TYPE W UMA CONTACT BINARIES

In previous studies, early-type and late-type EW binaries are usually separated on the basis of their period, with the early-type systems defined to have orbital periods $\log(P/d) > -0.25$ (e.g., Chen et al. 2018). It is also known that the early-type systems are fewer in number than the late-type systems (Pawlak 2016). Figure 5 shows the Wesenheit W_{JK} period-luminosity relationship (PLR) diagram for the EW binaries with classification probabilities of $\text{Prob} > 0.9$, $A_V < 1$ mag and $\text{parallax}/\text{parallax_error} > 10$. In the sample of ASAS-SN contact binaries, we immediately see that the slope of the late-type PLR is steeper than that of the early type systems. Pawlak (2016) studied a sample of early-type contact binaries in the Large Magellanic Cloud discovered by the OGLE survey (Graczyk et al. 2011; Pawlak et al. 2016) and noted that the PLR for contact binaries are best described by two separate relations for the late-type and early-type systems. He found a shallower slope for the early-type contact binaries when compared to the late-type PLR. The PLRs for late-type EW binaries have been extensively studied (Rucinski 1994; Chen et al. 2016, 2018).

While the traditional period for separating early and late type EW systems is at $\log(P/d) = -0.25$, the clear minimum in the period distribution (Figure 4) suggests that $\log(P/d) = -0.30$ is a better choice. In practice (see below), the two classes have some period overlap with early type systems having periods as short as $\log(P/d) = -0.40$ and late-type systems have periods as long as $\log(P/d) = -0.25$. Figure 5 shows the distribution of the systems in period and W_{JK} and, we see a clear break in the slope at a period of $\log(P/d) \sim -0.30$. We will fit models for the PLR in Section §4 after improving the separation between the early-type and late-type systems.

Jiang et al. (2014) found that the upper limit of the initial orbital period for binaries that come into contact ($\sim 3 - 4.2$ d) is significantly longer than the upper limit of the observed EW period distribution ($\sim 1 - 2$ d). Thus, the orbital period distribution for the EW binaries reflects significant orbital shrinkage compared to a zero-age binary population. This implies that the physics of the merger process must be responsible for shaping the observed PLRs of the early-type and late-type systems. A successful theory has to consider the evolution from a detached system to a contact system.

Figure 6 shows the distributions in effective temperature T_{eff} , surface gravity $\log(g)$ and metallicity $[\text{Fe}/\text{H}]$ for the early-type and late-type contact binaries with $\text{Prob} > 0.90$ in the APOGEE, LAMOST, GALAH and RAVE surveys. The distributions of the late-type ($N = 5248$) and early-type ($N = 888$) contact binaries in $\log(g)$ and $[\text{Fe}/\text{H}]$ are similar. There appears to be an excess of early-type binaries with $[\text{Fe}/\text{H}] < -0.8$. However, upon further inspection, we find that a substantial fraction of these low-metallicity sources are actually misclassified overtone RR Lyrae (RRc) variables that were assigned twice their true pulsational period in the ASAS-SN pipeline. RRc variables are sometimes confused with EW variables because of their symmetric light curve morphologies. We discard early-type binaries with $[\text{Fe}/\text{H}] < -0.8$ to minimize contamination.

The temperature distributions are, of course, quite different, but the separation of the two populations is very striking in the space of $\log(P/d)$ and T_{eff} , as shown in Figure 7. The increase in temperature with period is well known for the late-type systems, going back to the observation that longer period systems are bluer. The trend reverses for the late-type systems, which has not previously been observed. Qian et al. (2017) noted a trend but dismissed it as scatter. Still more striking is that there is a clean break between the two populations

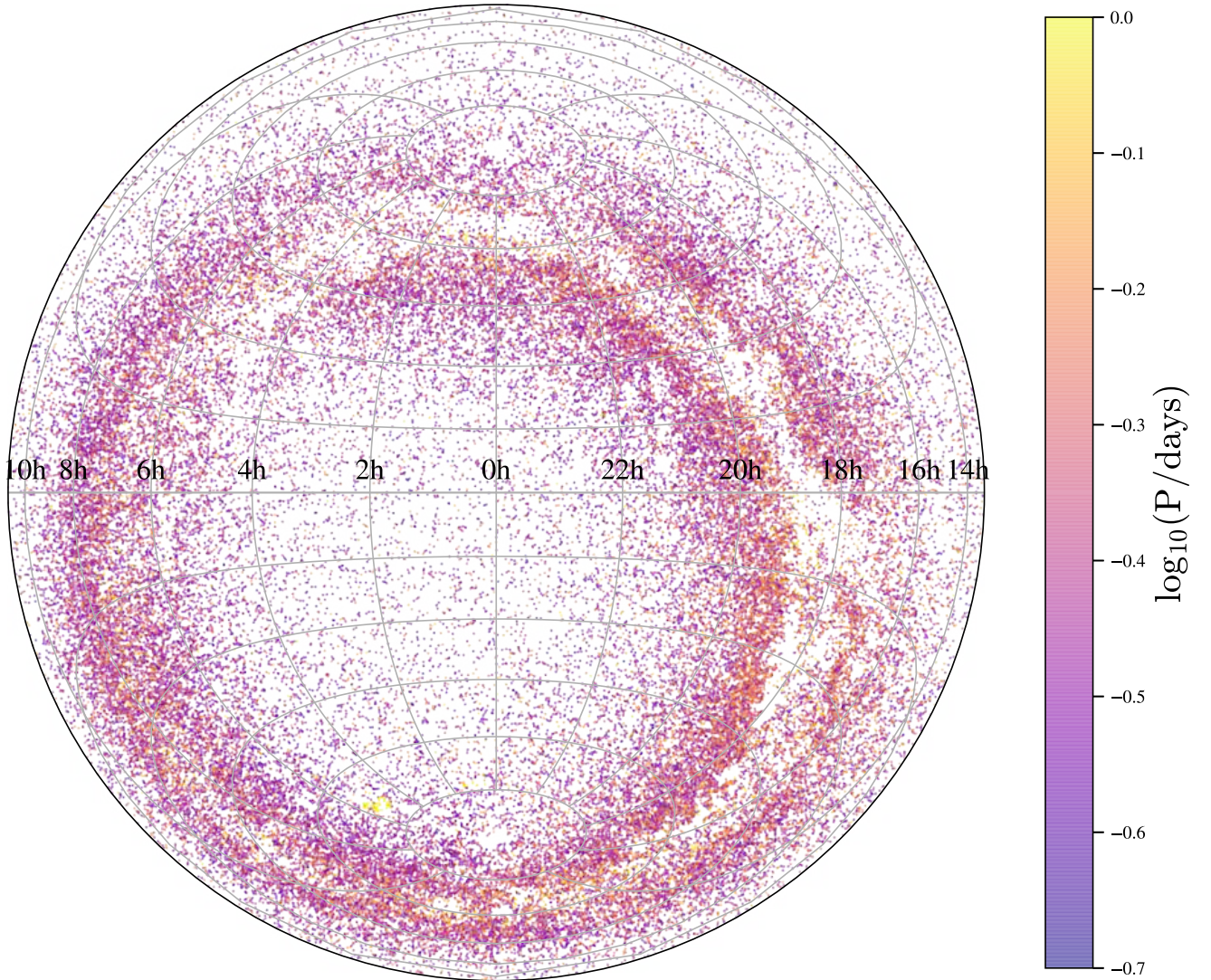


Figure 1. Projected distribution of the $\sim 71,200$ EW binaries in Equatorial coordinates (Lambert projection). The points are colored by period.

which we can empirically model as

$$T_{\text{eff}} = 6710\text{K} - 1760\text{K} \log(P/0.5\text{d}). \quad (2)$$

The traditional cut in period is an approximation to the actual separation of the two populations but a period separation of $\log(P/d) = -0.30$ at the minimum of the period distribution is a better “average” choice than the traditional $\log(P/d) = -0.25$. We use Equation 2 to separate the two populations in the spectroscopic sample.

The existence of the Kraft break (Kraft 1967) implies substantial changes in the envelope structure, winds and angular momentum loss for stars on the main-sequence. Stars above the Kraft break are hotter and rotate more rapidly than those below the Kraft break. The transition from slow to fast rotation occurs over the temperature range 6200 – 6700 K and it cannot be a coincidence that the split between early and late type contact binaries occurs at a similar temperature. Formation models for these systems generally invoke changes in the efficiency of angular momentum loss on the main sequence (Yildiz 2014) which is exactly the physics leading to the Kraft break. The remarkable feature of Figure 7 is the existence of a clear gap between

early and late type systems, which seems not to be predicted in any models.

If we separate the systems using Equation 2, we find period-temperature relations of

$$T_{\text{eff}}(\text{LT}) = 6598(\pm 23)\text{K} + 5260(\pm 116)\text{K} \log_{10}(P/0.5\text{d}), \quad (3)$$

for the late-type systems and

$$T_{\text{eff}}(\text{ET}) = 7041(\pm 28)\text{K} - 843(\pm 164)\text{K} \log_{10}(P/0.5\text{d}), \quad (4)$$

for the early-type systems. These relationships both have large scatter ($\sigma \gtrsim 300\text{K}$), but it is clear that the slopes are not only very different but reverse in sign (Figure 8). This can also be seen in the period-color distributions shown in Figure 9. Historically, the period-color relation of late-type systems have been well characterized (Eggen 1961, 1967). Here we see that the early-type systems become redder (cooler) with increasing orbital period, which is the reverse of the well-known correlations for the late-type systems.

Figure 10 shows the distribution of the spectroscopically classified systems in $\log(g)$ and $[\text{Fe}/\text{H}]$ versus temperature. For comparison,

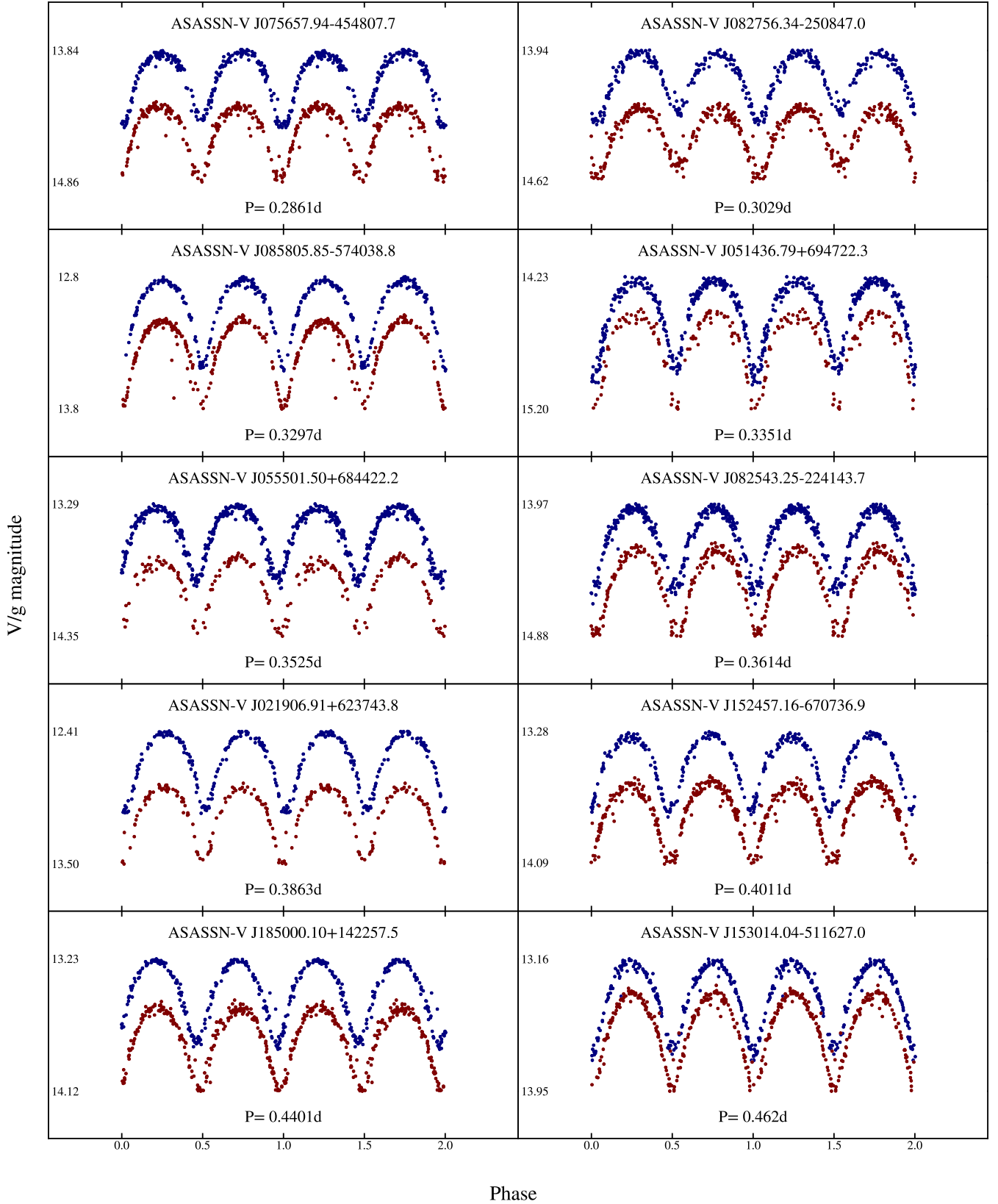


Figure 2. Phased ASAS-SN light curves for 10 late-type EW binaries. The light curves are scaled by their minimum and maximum V/g-band magnitudes. The blue (red) points are for the g(V) band data.

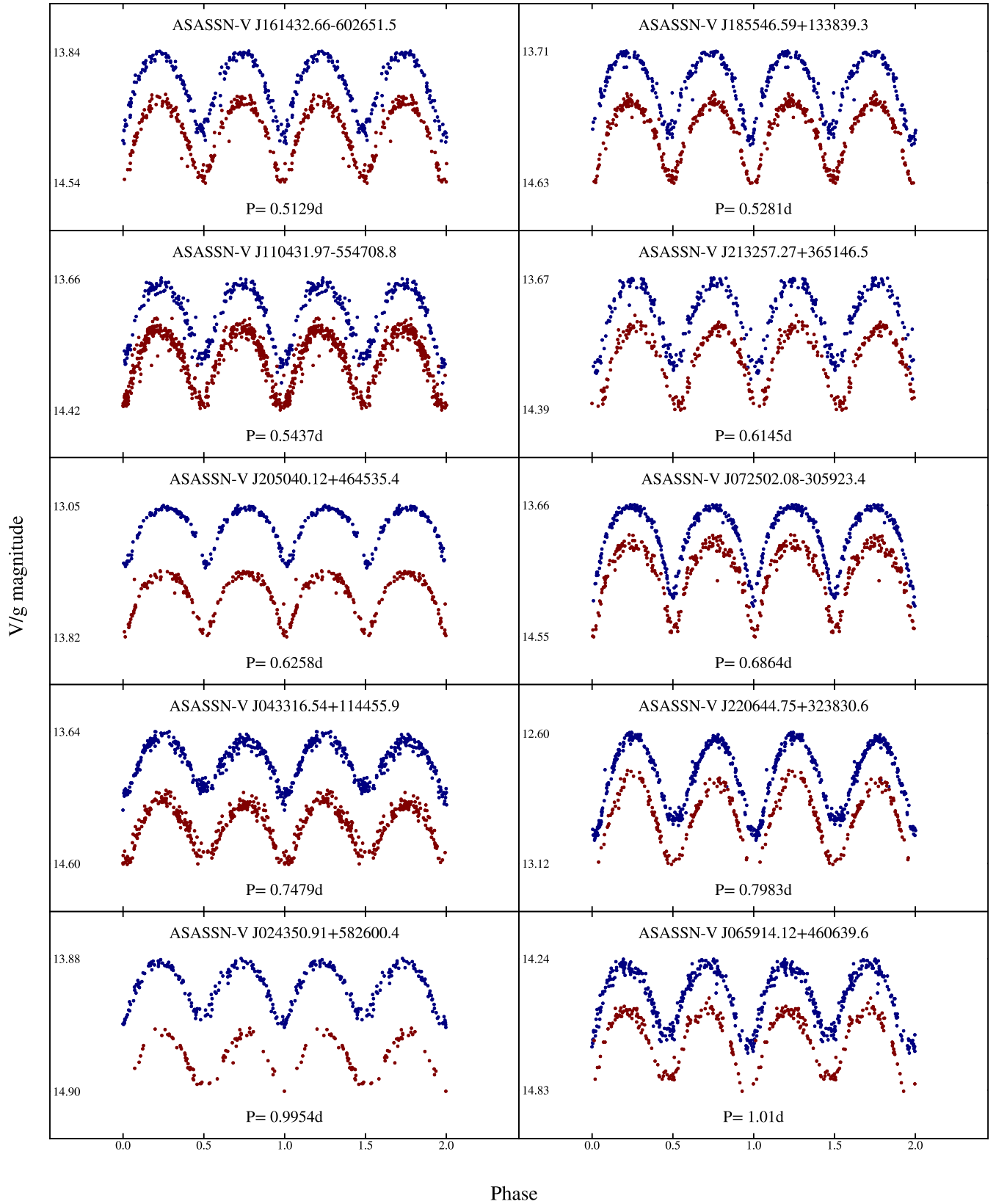


Figure 3. Phased ASAS-SN light curves for 10 early-type EW binaries. The format is the same as Figure 2.

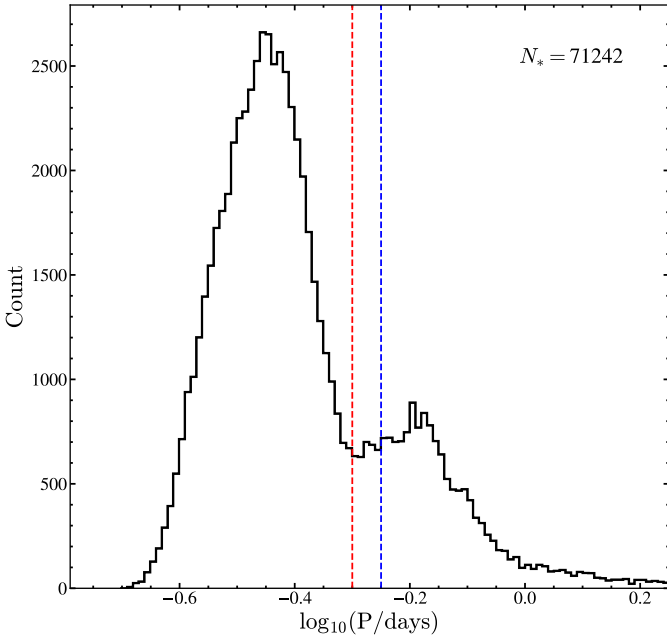


Figure 4. The distribution of orbital periods for the $\sim 71,200$ EW binaries. The usual period cut separating early-type and late-type systems of $\log(P/d) = -0.25$ is shown as a dashed blue line. A revised period cut of $\log(P/d) = -0.30$ based on the period distribution of the EW binaries in ASAS-SN is shown as a dashed red line.

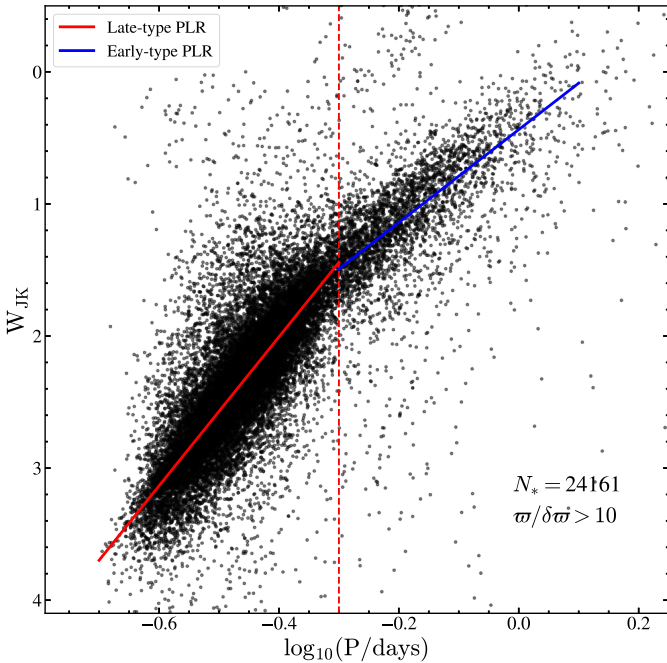


Figure 5. The Wesenheit W_{JK} PLR diagram for the EW stars with $\text{Prob} > 0.90$, $A_V < 1$ mag and parallaxes better than 10%. The fitted PLRs for the late-type and early-type contact binaries are shown as red and blue lines respectively.

we show MESA Isochrones and Stellar Tracks (MIST) isochrones (Choi et al. 2016; Dotter 2016) for single stars with $[\text{Fe}/\text{H}] = -0.25$ at 1 Gyr, 2 Gyr, 3 Gyr, 5 Gyr and 10 Gyr. The metallicity was chosen to match the median of the early-type systems. While using single star isochrones to interpret binaries combined with spectroscopic data models designed for single stars is risky, it is worth remembering that these systems basically have a single temperature. The most interesting feature of Figure 10 is probably that the systems have significantly lower $\log(g)$ than expected for main-sequence stars. For the higher mass systems, this could be due to evolution, but the effect is present even for the lower mass systems which should not have had time to evolve. The offset seems to be largest near the break temperature and smallest at higher and lower temperatures. El-Badry et al. (2018) did find that $\log(g)$ was moderately underestimated in fits of single star models to semi-empirical binary models and we also find that detached binaries have similar offsets in $\log(g)$. Non-variable single stars in the LAMOST survey have $\log(g)$ values consistent with models of main-sequence stars, so either the $\log(g)$ values are more biased than expected from El-Badry et al. (2018) or there is a genuine difference. There also appears to be a weak trend of the systems having higher metallicities at lower temperatures.

Figure 11 shows the early-type and late-type contact binaries with $A_V < 1$ mag and parallaxes better than 10% in a Gaia DR2 color-magnitude diagram (CMD) after correcting for interstellar extinction. A sample of nearby sources with good parallaxes and photometry is shown in the background. The isochrones do not track the main-sequence of the nearby stars as these have near-Solar metallicities while the isochrones are for a lower metallicity ($[\text{Fe}/\text{H}] = -0.25$). As expected, both groups of contact binaries are more luminous than stars on the main sequence and the early-type systems are more luminous than the late-type systems due to their higher masses.

Figure 12 shows the same early-type and late-type sources in Figure 11, colored by $\log(T_{\text{eff}})$. The average temperature of the early-type binaries drop with the perpendicular distance from the main sequence, thus, early-type binaries are cooler if they are further from the main-sequence. The late-type binaries do not show a similar gradient in temperature with the perpendicular distance from the main-sequence. The temperature simply increases with luminosity.

We use the empirical orbital period-mass relations derived in Gazeas & Stepień (2008) to derive estimates of the primary and secondary masses for the contact binaries with spectroscopic data. The masses derived from these relations have uncertainties of $\sim 15\%$. The 1%-99% quantile range of primary masses of the early-type and late-type systems were $1.27 - 3.29 M_{\odot}$ and $0.88 - 1.67 M_{\odot}$ respectively, whereas the distributions of secondary masses were $0.39 - 0.61 M_{\odot}$ and $0.33 - 0.44 M_{\odot}$ respectively. The total masses of the early-type and late-type systems were $1.66 - 3.90 M_{\odot}$ and $1.20 - 2.12 M_{\odot}$ respectively. The total masses of the W UMa binaries grow with the orbital period. These mass estimates are comparable to the theoretical estimates from Yıldız (2014). The median masses of the primaries for the early-type and late-type systems are $1.8 M_{\odot}$ and $1.2 M_{\odot}$ respectively. The masses of the primaries in the early-type (late-type) systems are consistent with their being above (below) the Kraft break. Simple main sequence lifetime arguments for the primaries of the early-type stars suggest that most of the sample should evolve off the main sequence at ~ 2 Gyr, whereas the majority of the primaries of the late-type stars should evolve off the main sequence at ~ 6 Gyr. This agrees with Figures 11 and 12, where the early-type systems seem to be more evolved.

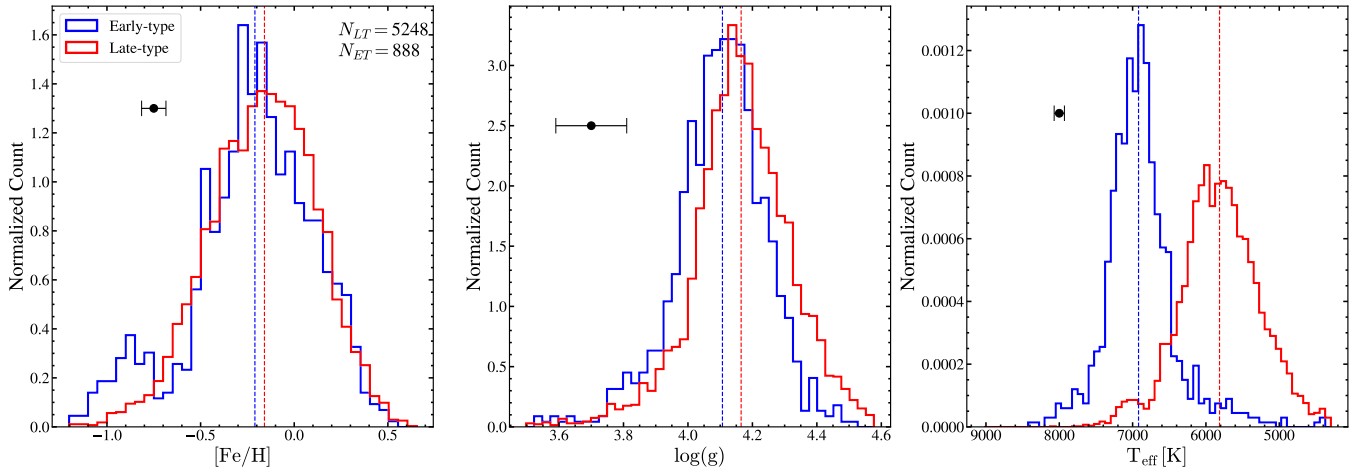


Figure 6. Distributions of the late-type (red) and early-type (blue) EW contact binaries with Prob > 0.90 in [Fe/H], log(*g*), and T_{eff} . The median value for each parameter is illustrated with a dashed line. The average uncertainty for each parameter is shown in black. The excess of early-type binaries with [Fe/H] < -0.8 is due to misclassified RRc variables.

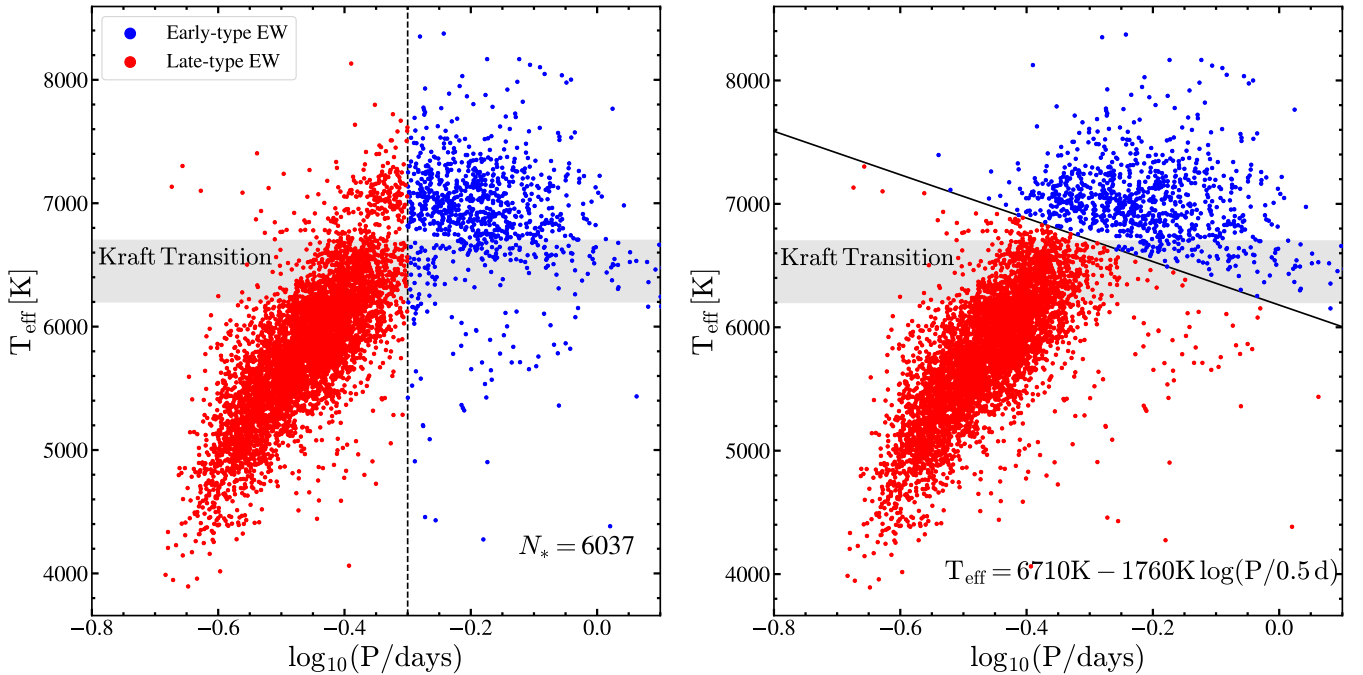


Figure 7. T_{eff} vs. log(*P*/*d*) for late-type (red) and early-type (blue) EW binaries separated by period (left) and a discriminant in T_{eff} -log(*P*/*d*) (right). The Kraft transition from slow to fast rotation occurs over the temperature range 6200 – 6700 K and is shaded in gray.

4 PERIOD-LUMINOSITY RELATIONS

PLRs exist only for late-type EW systems and are based on small samples (Rucinski 1994; Chen et al. 2018). Here we derive PLRs using much larger samples and for both early and late-type systems. We derive period-luminosity relations (PLRs) of the form

$$M_{\lambda} = A \log_{10}(P/0.5 \text{ d}) + B, \quad (5)$$

following the procedure in Jayasinghe et al. (2019e). We corrected for interstellar extinction with the SFD estimate. We include systems with `parallax/parallax_error` > 20, Prob > 0.98 and $A_V < 1$ mag to reduce the uncertainty in the absolute magnitudes. We made

an initial fit to each band, after which we removed outliers from the PLR fit by calculating the distance from the initial fit

$$r = \sqrt{(\Delta \log_{10} P)^2 + (\Delta M_{\lambda})^2},$$

where

$$\Delta \log_{10}(P) = \log_{10}(P_{\text{fit}}/P_{\text{obs}})$$

and

$$\Delta M_{\lambda} = M_{\lambda, \text{fit}} - M_{\lambda, \text{obs}}.$$

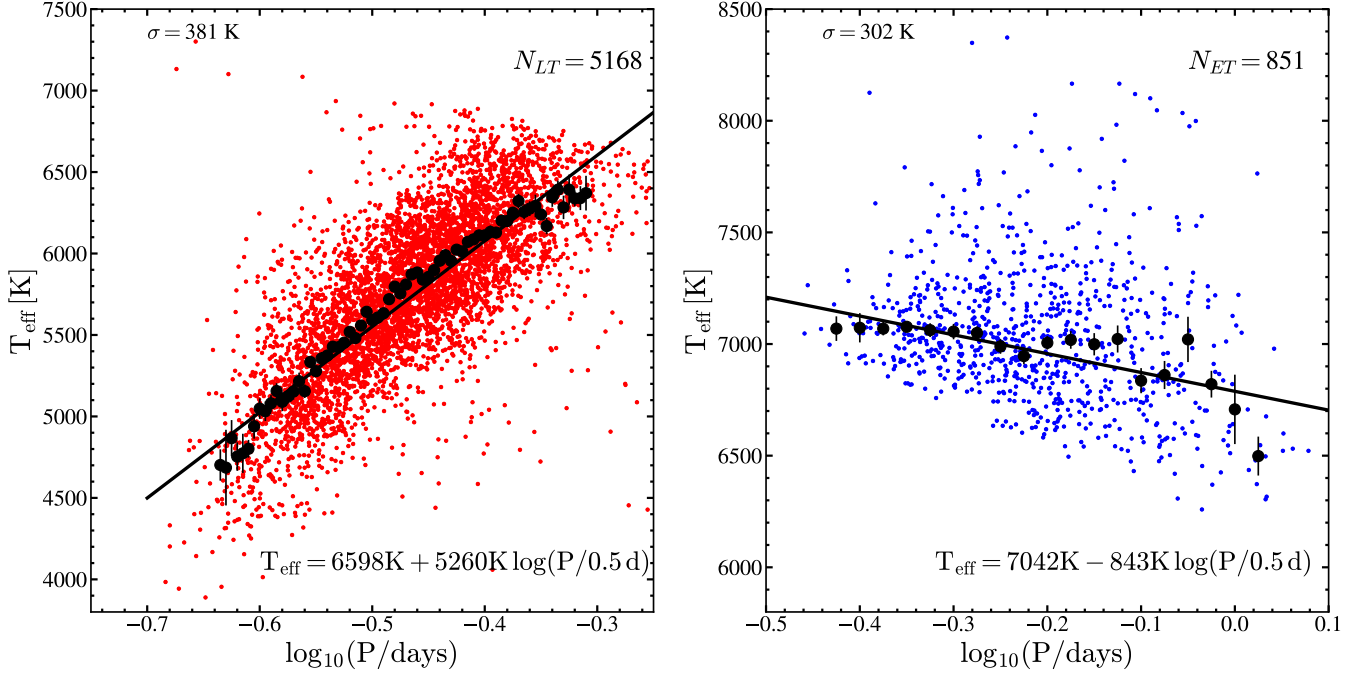


Figure 8. T_{eff} vs. $\log(P/d)$ for the late-type (left) and early-type (right) EW binaries. Linear fits to the binned data are shown in black.

Sources that deviated from this fit by $> 2\sigma_r$ were removed. After removing these outliers, the parameters from the trial fit were then used to initialize a Monte Carlo Markov Chain sampler (MCMC) with 200 walkers, that were run for 20000 iterations using the MCMC implementation *emcee* (Foreman-Mackey et al. 2013). The errors in the PLR parameters were derived from the MCMC chains. Since we are using photometry obtained at random phases, these PLRs essentially correspond to the PLRs for the mean magnitudes of the binaries. However, they will have an additional scatter of ~ 0.05 mag because they are not individually averaged (or peak) magnitudes for each binary (Chen et al. 2018). For the early-type binaries, we only use the spectroscopic sample to avoid contamination by both late-type binaries and RRc variables, while for the late-type binaries, we augment the sample by including sources with $\log(P/d) < -0.4$ where there is no confusion between late-type and early-type contact binaries (Figure 7).

Given that most EW binaries do not have spectroscopic data to separate early-type and late-type systems based on equation 2, we also derive PLRs for early-type and late-type systems separated by period. Figure 13 shows the period distribution of the early-type and late-type systems with spectroscopic information. To separate these systems based only on their orbital period, we use the cutoff of $\log(P/d) = -0.30$ at the minimum of the period distribution in Figure 5. We chose the cut based on the orbital period distribution of the $\sim 71,200$ EW binaries in ASAS-SN, instead of deriving a different cut from Figure 13 because it could be biased by selection effects in the spectroscopic sample. The usual cut of $\log(P/d) = -0.25$ excludes a significant number of shorter period early-type systems, but it does provide a clean sample of longer period early-type systems. The best-fit parameters, their uncertainties, the dispersion, and the number of sources used in the fit are listed in Table 1 (late-type) and Table 2 (early-type) for the EW binaries separated in period-temperature space, and in Table 3 (late-type) and Table 4 (early-type) for the EW binaries separated by period.

Figure 14 illustrates the PLRs of the late-type and early-type systems separated in period-temperature space. The PLR slopes are significantly different for the early-type and late-type binaries. The PLR slopes for the late-type systems separated in period-temperature space also differ by $\lesssim 1\%$ from the PLR slopes of the late-type systems separated by period. The slopes for the late-type systems derived with these two samples are consistent given the errors. On the other hand, early-type systems have slopes that differ by $\sim 1\%$ in the V-band and $\sim 25\%$ in the K_s -band. The NIR PLR slopes for the early-type systems between the two ways of separating the EW sub-types are inconsistent given their uncertainties. The slopes of the PLR fits for the late-type binaries differ by $> 3\sigma$ with those obtained by Chen et al. (2018), but the disagreement is smaller for the NIR PLRs. For example, their V-band (-9.14 ± 0.40) and K_s -band (-5.95 ± 0.21) slopes are shallower than the slopes derived here by $\sim 14\%$ and $\sim 7\%$ respectively. In addition, at the median period $P \sim 0.34$ d of the late-type EW binaries, the PLR fits differ by ~ 0.3 mag in the V-band and ~ 0.1 mag in the K_s -band from those obtained by Chen et al. (2018). These differences are smaller than the scatter in the PLRs at these bands. Chen et al. (2018) derived PLRs for the late-type contact binaries based on a small sample of only 183 nearby ($d < 330$ pc) sources with an average extinction of $A_V = 0.075 \pm 0.025$ mag, whereas our PLR fits are made to a much bigger sample ($\sim 61\times$) across a wider range in distance and A_V . There are no significant changes in the PLR fits if we restrict our sample to smaller extinctions ($A_V < 0.5$ mag). Contact binaries are more diverse and span a much larger range in luminosity and temperature than classical pulsators like RR Lyrae and Cepheids, leading to more dispersion about the PLR.

5 CONCLUSIONS

We analyzed a sample of 71242 W UMa eclipsing binaries, including 12584 new discoveries, in the ASAS-SN V-band catalog of variable

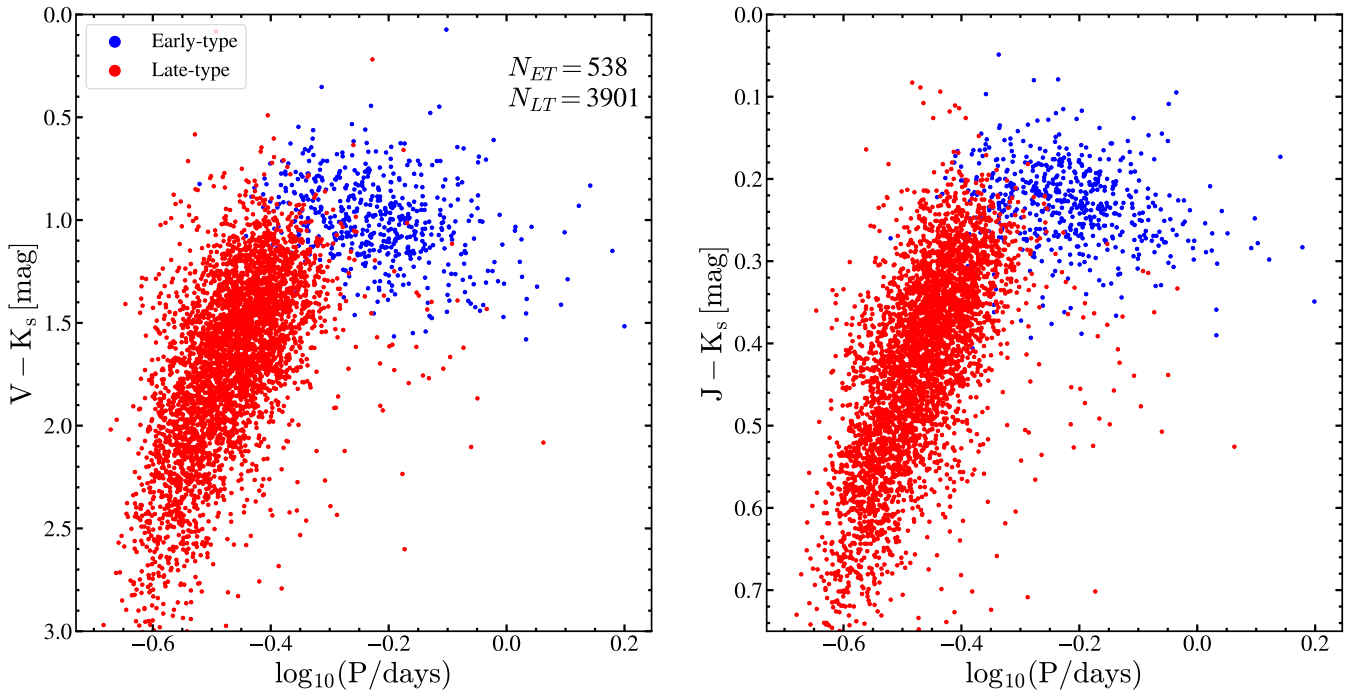


Figure 9. $V - K_s$ (left) and $J - K_s$ (right) vs. $\log(P/d)$ for the spectroscopically separated late-type (red) and early-type (blue) EW binaries separated in period-temperature space using equation 2, with $\text{Prob} > 0.9$ and $A_V < 0.5$ mag.

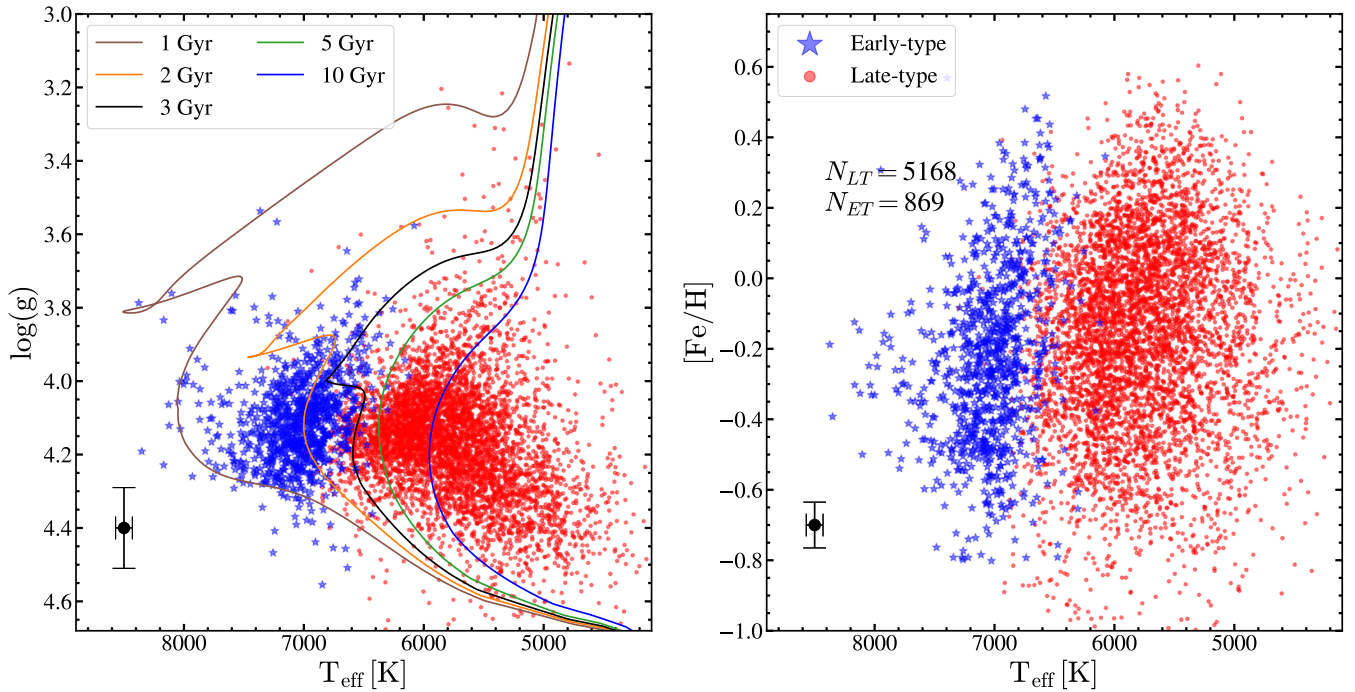


Figure 10. Distributions of the early-type and late-type contact binaries in $\log(g)$ vs. T_{eff} (left) and T_{eff} vs. $[\text{Fe}/\text{H}]$ (right). MIST isochrones (Choi et al. 2016; Dotter 2016) for single stars with $[\text{Fe}/\text{H}] = -0.25$ at 1 Gyr, 2 Gyr, 3 Gyr, 5 Gyr and 10 Gyr are shown for comparison. The average uncertainties are shown by the black error bars.

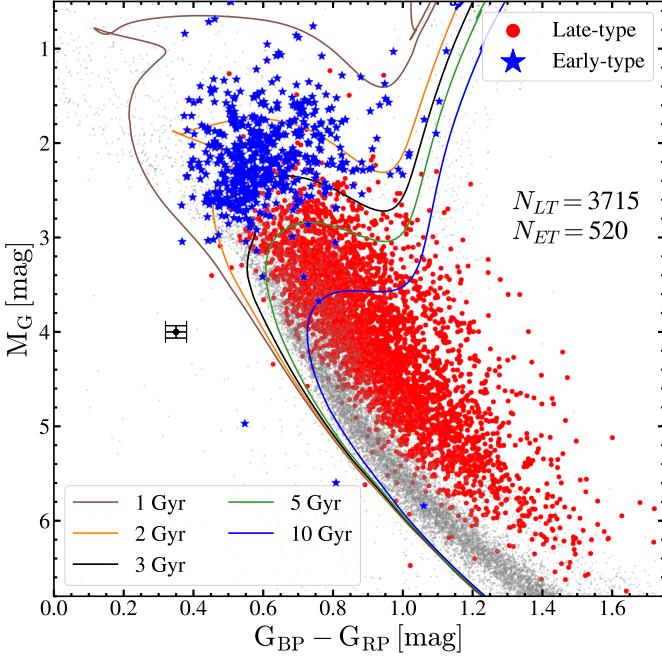


Figure 11. Gaia DR2 color-magnitude diagram for a sample of the early-type (blue) and late-type (red) EW binaries with Prob > 0.90, $A_V < 1$ mag and parallaxes better than 10%, which were separated in period-temperature space using Equation 2. A sample of nearby sources with good parallaxes and photometry is shown in gray. MIST isochrones (Choi et al. 2016; Dotter 2016) for single stars with $[\text{Fe}/\text{H}] = -0.25$ at 1 Gyr, 2 Gyr, 3 Gyr, 5 Gyr and 10 Gyr are shown for comparison. The average uncertainties are shown by the black error bars. Solar metallicity MIST isochrones lie on the gray points.

Table 1. PLR parameters for the late-type contact binaries separated in period-temperature space

Band	A mag	B mag	σ mag	N
W_{JK}	-5.527 ± 0.052	1.469 ± 0.049	0.197	11384
V	-10.628 ± 0.052	2.360 ± 0.054	0.383	11134
G	-10.173 ± 0.047	2.379 ± 0.050	0.337	11329
J	-7.651 ± 0.049	1.763 ± 0.054	0.254	11363
H	-6.589 ± 0.047	1.623 ± 0.048	0.222	11414
K_s	-6.381 ± 0.051	1.601 ± 0.045	0.214	11387
W_1	-6.369 ± 0.051	1.540 ± 0.051	0.199	11579

Table 2. PLR parameters for the early-type contact binaries separated in period-temperature space

Band	A mag	B mag	σ mag	N
W_{JK}	-3.616 ± 0.048	1.499 ± 0.049	0.140	226
V	-2.770 ± 0.049	2.407 ± 0.051	0.166	221
G	-2.977 ± 0.047	2.426 ± 0.049	0.154	228
J	-3.512 ± 0.050	1.799 ± 0.049	0.144	226
H	-3.535 ± 0.050	1.650 ± 0.050	0.145	231
K_s	-3.520 ± 0.051	1.612 ± 0.043	0.142	228
W_1	-3.565 ± 0.056	1.583 ± 0.045	0.129	234

Table 3. PLR parameters for the late-type contact binaries separated by period

Band	A mag	B mag	σ mag	N
W_{JK}	-5.523 ± 0.049	1.482 ± 0.059	0.195	11118
V	-10.531 ± 0.047	2.373 ± 0.047	0.378	10843
G	-10.076 ± 0.047	2.410 ± 0.057	0.331	11007
J	-7.678 ± 0.046	1.753 ± 0.051	0.251	11089
H	-6.612 ± 0.048	1.619 ± 0.054	0.220	11148
K_s	-6.402 ± 0.044	1.581 ± 0.053	0.212	11123
W_1	-6.359 ± 0.055	1.545 ± 0.055	0.197	11300

Table 4. PLR parameters for the early-type contact binaries separated by period

Band	A mag	B mag	σ mag	N
W_{JK}	-2.640 ± 0.051	1.403 ± 0.059	0.258	1199
V	-2.753 ± 0.049	2.328 ± 0.047	0.351	1176
G	-2.772 ± 0.049	2.379 ± 0.051	0.334	1186
J	-2.635 ± 0.051	1.716 ± 0.050	0.284	1189
H	-2.675 ± 0.048	1.575 ± 0.053	0.271	1198
K_s	-2.656 ± 0.051	1.528 ± 0.054	0.269	1203
W_1	-2.709 ± 0.055	1.487 ± 0.060	0.250	1192

stars, taking advantage of their Gaia DR2 parallaxes (Gaia Collaboration et al. 2018a) and the spectroscopic temperatures, metallicities and $\log(g)$ estimates from primarily LAMOST, but also GALAH, RAVE and APOGEE, for 7169 of the stars. The large sample size and (in particular) the spectroscopic temperatures lead to a much clearer view of the dichotomy between early and late-type systems. The period distribution has a clear minimum at $\log(P/d) = -0.30$, making it a better separator between the two populations than the standard of $\log(P/d) = -0.25$. The period-luminosity relation also has a distinct break in its slope at the same period.

The distinction between the populations is even clearer in the space of period and effective temperature, where there is essentially a gap along the line $T_{\text{eff}} = 6710\text{K} - 1760\text{K} \log(P/0.5\text{d})$. There are no strong distinctions between the populations in metallicity or $\log(g)$, nor strong correlations within the populations with these properties. Early-type systems are hotter at shorter orbital periods and get cooler as the orbital period increases. The total mass of the EW binaries increases with their orbital period. Thus more massive early-type EW are cooler and likely more evolved than the less massive early-type EW that are hotter.

With the larger number of systems and a clearer separation of the two classes, we then derive revised period-luminosity relations for the late-type and early-type EW binaries in the W_{JK} , V , Gaia DR2 G , J , H , K_s and W_1 bands for contact binaries both separated spectroscopically and by period. The slopes of the late-type PLRs for the two ways of dividing the systems were consistent with each other given the uncertainties, but the slopes of the early-type PLRs differ by $\sim 25\%$ in the NIR. The slopes we find for late-type PLRs differ significantly ($\sim 10\%$) from the existing PLRs for late-type EW binaries given their uncertainties. This is likely due to the far smaller samples used by previous studies to derive PLRs.

The Kraft break appears to determine the observed dichotomy of the contact binaries. Stars lose angular momentum inefficiently above the Kraft break, making it unlikely that angular momentum loss is sufficient to bring the early-type systems into contact. Thus,

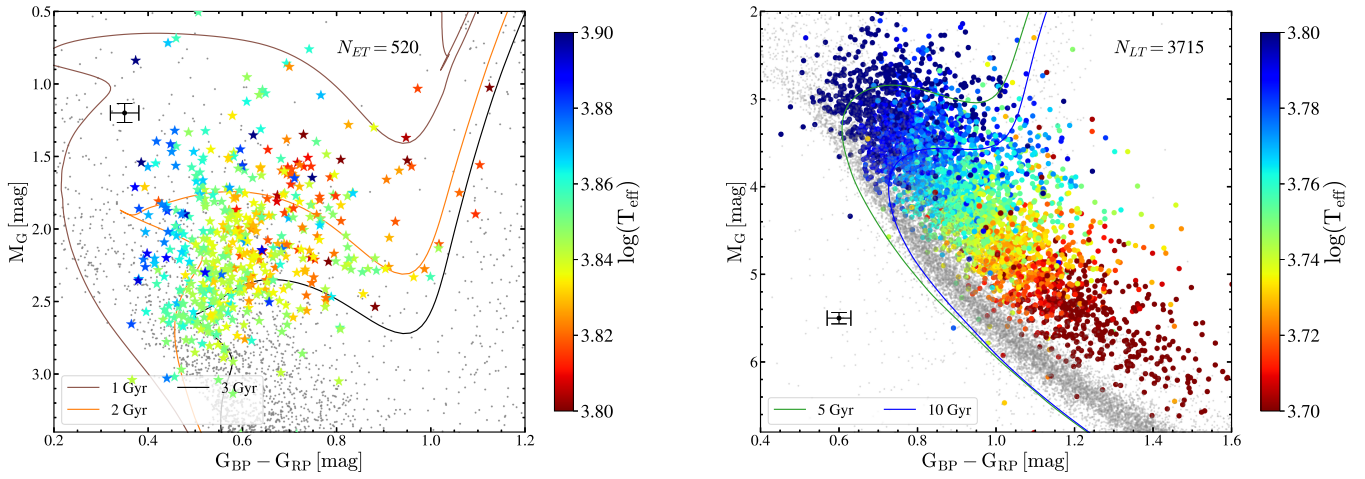


Figure 12. Gaia DR2 color-magnitude diagrams for the early-type (left) and late-type (right) EW binaries shown in Figure 11, colored by $\log(T_{\text{eff}})$. The colorbars show the same dynamic range in $\log(T_{\text{eff}})$ of 0.1 dex. A sample of nearby sources with good parallaxes and photometry is shown in gray. MIST isochrones (Choi et al. 2016; Dotter 2016) for single stars with $[\text{Fe}/\text{H}] = -0.25$ at 1 Gyr, 2 Gyr, 3 Gyr, 5 Gyr and 10 Gyr are shown for comparison. The average uncertainties are shown by the black error bars.

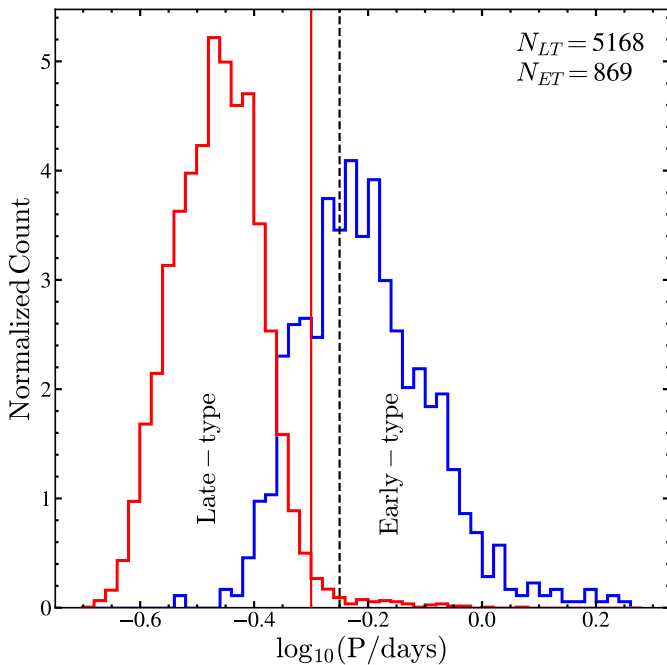


Figure 13. The distribution of orbital periods for the early-type (blue) and late-type (red) EW binaries which were separated in period-temperature space using Equation 2. The usual period cut separating early-type and late-type systems of $\log(P/d) = -0.25$ is shown as a dashed black line. The suggested period cut of $\log(P/d) = -0.30$ for separating the systems is shown as a solid red line.

early-type systems form due to stellar evolution and the subsequent expansion of a more massive component that is above the Kraft break ($\sim 1.3M_{\odot}$). For the late-type systems, the primary is below the Kraft break, and the late-type systems can come into contact due to efficient angular momentum loss during the detached phase. The positions of the EW binaries on a Gaia DR2 color-magnitude diagram are consistent with early-type EW binaries being younger

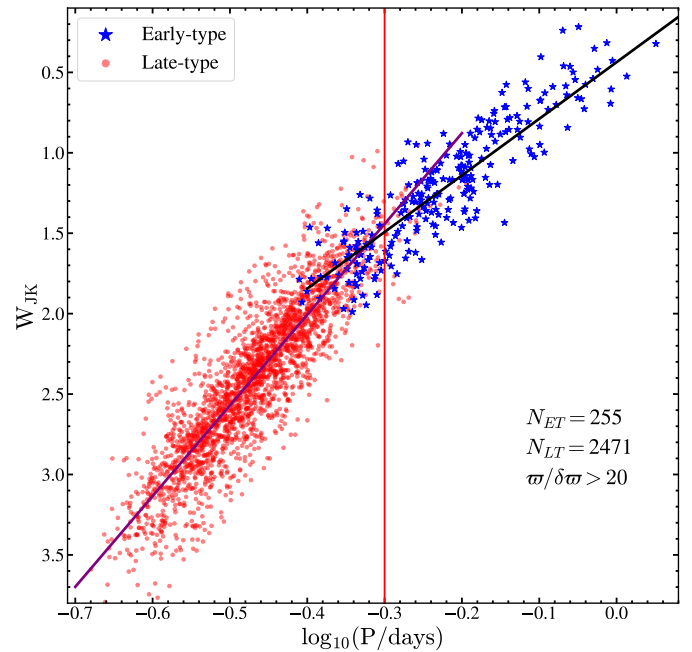


Figure 14. The Wesenheit W_{JK} PLR diagram for the EW stars separated in period-temperature space using Equation 2, with $\text{Prob} > 0.98$, $A_V < 1$ mag and parallaxes better than 5% after clipping outliers with dispersions $> 3\sigma_r$ from the respective PLR fit. The fitted PLRs for the late-type and early-type contact binaries are shown as purple and black lines respectively. The suggested period cut of $\log(P/d) = -0.30$ for separating the systems is shown as a solid red line.

and more evolved than the late-type systems. Late-type EW binaries appear to be main sequence binaries and the vast majority of these appear older than 5 Gyr. This is consistent with standard models for the formation and evolution of these systems (Yildiz 2014; Jiang et al. 2014).

ACKNOWLEDGEMENTS

We thank the referee, Dr. Diana Kjurkchieva, for the very useful comments that improved our presentation of this work. We thank Dr. Jennifer Johnson for useful discussions on this manuscript. We thank the Las Cumbres Observatory and its staff for its continuing support of the ASAS-SN project. We also thank the Ohio State University College of Arts and Sciences Technology Services for helping us set up and maintain the ASAS-SN variable stars and photometry databases.

ASAS-SN is supported by the Gordon and Betty Moore Foundation through grant GBMF5490 to the Ohio State University, and NSF grants AST-1515927 and AST-1908570. Development of ASAS-SN has been supported by NSF grant AST-0908816, the Mt. Cuba Astronomical Foundation, the Center for Cosmology and AstroParticle Physics at the Ohio State University, the Chinese Academy of Sciences South America Center for Astronomy (CAS- SACA), the Villum Foundation, and George Skestos.

KZS and CSK are supported by NSF grants AST-1515927, AST-1814440, and AST-1908570. BJS is supported by NSF grants AST-1908952, AST-1920392, and AST-1911074. TAT acknowledges support from a Simons Foundation Fellowship and from an IBM Einstein Fellowship from the Institute for Advanced Study, Princeton. Support for JLP is provided in part by the Ministry of Economy, Development, and Tourism's Millennium Science Initiative through grant IC120009, awarded to The Millennium Institute of Astrophysics, MAS. Support for MP and OP has been provided by INTER-EXCELLENCE grant LTAUSA18093 from the Czech Ministry of Education, Youth, and Sports. The research of OP has also been supported by Horizon 2020 ERC Starting Grant "Cat-In-hAT" (grant agreement #803158) and PRIMUS/SCI/17 award from Charles University. This work was partly supported by NSFC 11721303.

This work has made use of data from the European Space Agency (ESA) mission *Gaia* (<https://www.cosmos.esa.int/gaia>), processed by the *Gaia* Data Processing and Analysis Consortium. This publication makes use of data products from the Two Micron All Sky Survey, as well as data products from the Wide-field Infrared Survey Explorer. This research was also made possible through the use of the AAVSO Photometric All-Sky Survey (APASS), funded by the Robert Martin Ayers Sciences Fund.

This research has made use of the VizieR catalogue access tool, CDS, Strasbourg, France. This research also made use of Astropy, a community-developed core Python package for Astronomy (Astropy Collaboration, 2013).

REFERENCES

Alard, C. 2000, *A&AS*, 144, 363
 Alard, C., & Lupton, R. H. 1998, *ApJ*, 503, 325
 Alcock, C., Allsman, R. A., Alves, D., et al. 1997, *ApJ*, 486, 697
 Andronov, N., Pinsonneault, M. H., & Terndrup, D. M. 2006, *ApJ*, 646, 1160
 Astropy Collaboration, Robitaille, T. P., Tollerud, E. J., et al. 2013, *A&A*, 558, A33
 Bailor-Jones, C. A. L., Rybizki, J., Fouesneau, M., Mantelet, G., & Andrae, R. 2018, *AJ*, 156, 58
 Bhatti, W., Bouma, L. G., Wallace, J., et al. 2018, *astrobase*, v0.3.8, Zenodo, <http://doi.org/10.5281/zenodo.1185231>
 Binnendijk, L. 1970, *Vistas in Astronomy*, 12, 217
 Buder, S., Asplund, M., Duong, L., et al. 2018, *MNRAS*, 478, 4513
 Casey, A. R., Hawkins, K., Hogg, D. W., et al. 2017, *ApJ*, 840, 59
 Cardelli, J. A., Clayton, G. C., & Mathis, J. S. 1989, *ApJ*, 345, 245
 Chen, X., & Han, Z. 2009, *MNRAS*, 395, 1822
 Chen, X., de Grijs, R., & Deng, L. 2016, *ApJ*, 832, 138

Chen, X., Deng, L., de Grijs, R., et al. 2018, *ApJ*, 859, 140
 Choi, J., Dotter, A., Conroy, C., et al. 2016, *ApJ*, 823, 102
 Cutri, R. M., & et al. 2013, *VizieR Online Data Catalog*, 2328,
 Cui, X.-Q., Zhao, Y.-H., Chu, Y.-Q., et al. 2012, *Research in Astronomy and Astrophysics*, 12, 1197
 de Mink, S. E., Langer, N., Izzard, R. G., et al. 2013, *ApJ*, 764, 166
 De Silva, G. M., Freeman, K. C., Bland-Hawthorn, J., et al. 2015, *MNRAS*, 449, 2604
 Derue, F., Marquette, J.-B., Lupone, S., et al. 2002, *A&A*, 389, 149
 Dotter, A. 2016, *ApJS*, 222, 8
 Drake, A. J., Graham, M. J., Djorgovski, S. G., et al. 2014, *ApJS*, 213, 9
 Eggen, O. J. 1961, *Royal Greenwich Observatory Bulletins*, 31, 101
 Eggen, O. J. 1967, *Mem. RAS*, 70, 111
 Eggleton, P. P. 1983, *ApJ*, 268, 368
 Eggleton, P. P., & Kiseleva-Eggleton, L. 2001, *ApJ*, 562, 1012
 Eggleton, P. P. 2010, *New Astron. Rev.*, 54, 45
 Eker, Z., Demircan, O., Bilir, S., et al. 2006, *MNRAS*, 373, 1483
 El-Badry, K., Ting, Y.-S., Rix, H.-W., et al. 2018, *MNRAS*, 476, 528
 Flannery, B. P. 1976, *ApJ*, 205, 217
 Foreman-Mackey, D., Hogg, D. W., Lang, D., et al. 2013, *PASP*, 125, 306
 Gaia Collaboration, Brown, A. G. A., Vallenari, A., et al. 2018, *arXiv:1804.09365*
 Gaia Collaboration, Eyer, L., Rimoldini, L., et al. 2018, *arXiv:1804.09382*
 Gaia Collaboration, Helmi, A., van Leeuwen, F., et al. 2018, *A&A*, 616, A12.
 Gazeas, K., & Stępień, K. 2008, *MNRAS*, 390, 1577
 Graczyk, D., Soszyński, I., Poleski, R., et al. 2011, *Acta Astron.*, 61, 103
 Heinze, A. N., Tonry, J. L., Denneau, L., et al. 2018, *arXiv:1804.02132*
 Henden, A. A., Levine, S., Terrell, D., & Welch, D. L. 2015, *American Astronomical Society Meeting Abstracts*
 Holtzman, J. A., Shetrone, M., Johnson, J. A., et al. 2015, *AJ*, 150, 148
 Jayasinghe, T., Kochanek, C. S., Stanek, K. Z., et al. 2018, *MNRAS*, 477, 3145
 Jayasinghe, T., Stanek, K. Z., Kochanek, C. S., et al. 2019, *MNRAS*, 486, 1907
 Jayasinghe T., et al., 2019, *MNRAS*, 485, 961
 Jayasinghe, T., Stanek, K. Z., Kochanek, C. S., et al. 2019, *MNRAS*, 2120
 Jayasinghe, T., Stanek, K. Z., Kochanek, C. S., et al. 2019, *arXiv e-prints*, *arXiv:1907.10609*
 Jayasinghe, T., Stanek, K. Z., Kochanek, C. S., et al. 2019, *arXiv e-prints*, *arXiv:1910.14187*
 Jiang, D., Han, Z., & Li, L. 2014, *MNRAS*, 438, 859
 Kochanek, C. S., Shappee, B. J., Stanek, K. Z., et al. 2017, *PASP*, 129, 104502
 Kovács, G., Zucker, S., & Mazeh, T. 2002, *A&A*, 391, 369
 Kozai, Y. 1962, *AJ*, 67, 591
 Kraft, R. P. 1967, *ApJ*, 150, 551
 Lebzelter, T., Mowlavi, N., Marigo, P., et al. 2018, *arXiv:1808.03659*
 Li, L., Zhang, F., Han, Z., et al. 2007, *ApJ*, 662, 596
 Lidov, M. L. 1962, *Planet. Space Sci.*, 9, 719
 Lucy, L. B. 1976, *ApJ*, 205, 208
 Madore, B. F. 1982, *ApJ*, 253, 575
 Majewski, S. R., Schiavon, R. P., Frinchaboy, P. M., et al. 2017, *AJ*, 154, 94
 Paczyński, B., Szczygieł, D. M., Pilecki, B., et al. 2006, *MNRAS*, 368, 1311
 Pawlak, M., Soszyński, I., Udalski, A., et al. 2016, *Acta Astron.*, 66, 421
 Pawlak, M. 2016, *MNRAS*, 457, 4323
 Pojmanski, G. 2002, *Acta Astron.*, 52, 397
 Qian, S.-B., He, J.-J., Zhang, J., et al. 2017, *Research in Astronomy and Astrophysics*, 17, 087
 Royer, F., Zorec, J., & Gómez, A. E. 2007, *A&A*, 463, 671
 Rucinski, S. M. 1974, *Acta Astron.*, 24, 119
 Rucinski, S. M. 1986, *Instrumentation and Research Programmes for Small Telescopes*, 159
 Rucinski, S. M. 1994, *PASP*, 106, 462
 Rucinski, S. M. 1997, *AJ*, 113, 407
 Rucinski, S. M. 2006, *MNRAS*, 368, 1319
 Samus, N. N., Kazarovets, E. V., Durlevich, O. V., et al. 2017, *Astronomy Reports*, 61, 80
 Scargle, J. D. 1982, *ApJ*, 263, 835
 Schlafly, E. F., & Finkbeiner, D. P. 2011, *ApJ*, 737, 103

- Schlegel, D. J., Finkbeiner, D. P., & Davis, M. 1998, *ApJ*, 500, 525
Shappee, B. J., Prieto, J. L., Grupe, D., et al. 2014, *ApJ*, 788, 48
Skrutskie, M. F., Cutri, R. M., Stiening, R., et al. 2006, *AJ*, 131, 1163
Taylor, M. B. 2005, *Astronomical Data Analysis Software and Systems XIV*, 347, 29
Tonry, J. L., Denneau, L., Heinze, A. N., et al. 2018, *PASP*, 130, 064505
Tonry, J. L., Denneau, L., Flewelling, H., et al. 2018, *ApJ*, 867, 105
Tylenda, R., Hajduk, M., Kamiński, T., et al. 2011, *A&A*, 528, A114
Udalski, A. 2003, *Acta Astron.*, 53, 291
Vilhu, O. 1982, *A&A*, 109, 17
van Eyken, J. C., Ciardi, D. R., Rebull, L. M., et al. 2011, *AJ*, 142, 60
van Saders, J. L., & Pinsonneault, M. H. 2013, *ApJ*, 776, 67
Watson, C. L., Henden, A. A., & Price, A. 2006, *Society for Astronomical Sciences Annual Symposium*, 25, 47
Webbink, R. F. 1976, *ApJS*, 32, 583
Webbink, R. F. 2003, *3D Stellar Evolution*, 76
Wright, E. L., Eisenhardt, P. R. M., Mainzer, A. K., et al. 2010, *AJ*, 140, 1868
Woźniak, P. R., Vestrand, W. T., Akerlof, C. W., et al. 2004, *AJ*, 127, 2436
Yakut, K., & Eggleton, P. P. 2005, *ApJ*, 629, 1055
Yildiz, M. 2014, *MNRAS*, 437, 185
Yildiz, M., & Doğan, T. 2013, *MNRAS*, 430, 2029
Zechmeister, M., & Kürster, M. 2009, *A&A*, 496, 577

This paper has been typeset from a $\text{\TeX}/\text{\LaTeX}$ file prepared by the author.